Dijlah Journal of Engineering Science (DJES) Vol. 3, No. 1, March, 2026, pp.209-224
ISSN: Printed: **3078-9656, Online: 3078-9664**, paper ID: 125

Improving the efficiency of thermal-to-electricity conversion using integrated heat exchange technologies in small systems

Mohammed Saad Kamil[1]
[1]Research and Technology Azarbaijan Shahid Madani University, Department of Mechanics in Partial Fulfillment, Iran

Article Info

Article history:

Received Nov., 16, 2025
Revised Nov.,20, 2025
Accepted Dec.,15, 2025

Keywords:

Thermal-to-electric energy conversion
Heat exchange
Nanogenerators
Internet of Things (IoT)
Energy efficiency
Small-scale systems
Sustainable energy

ABSTRACT

This research aims to investigate the enhancement of thermal-to-electricity conversion efficiency using integrated heat exchange technologies in small-scale systems, in light of the growing global interest in sustainable energy sources and their role in powering Internet of Things (IoT) devices and self-sustained systems. The study reviews the theoretical foundations of thermal energy conversion through thermoelectric and pyroelectric nanogenerators, while analyzing the contribution of integrated heat exchangers in improving system efficiency and reducing thermal losses. Furthermore, it highlights recent models of miniaturized heat exchangers and performance optimization strategies based on advanced materials and innovative structural designs. The findings suggest that combining nanotechnology with integrated heat exchange significantly enhances thermal-to-electric conversion efficiency, paving the way for practical applications in smart sensing, wearable devices, and low-power embedded systems.

Corresponding Author:

Mohammed Saad Kamil1
Research and Technology Azarbaijan Shahid Madani University, Department of Mechanics in Partial Fulfillment, Iran
Email: Kamilmohammedsaad@gmail.com

1. INTRODUCTION

Altering wasted environmental energy into available electric power has been an out-of-reach source of electricity for the long-compatibility Internet of Things systems. The technological advancements have significantly decreased the massive amount of electricity that IoT systems devoured. It still cannot present an equivalent solution for this amidst the electricity consumption. This is “the part” of harvesting environmental energy that is thrown into waste, and nothing else can be displayed. Wasted environmental energy alterations have emerged as a major benefit in long-compatibility Internet of Things systems. Otherwise, thermoelectricity could be another potential electricity-harvesting opportunity. The pyroelectric effect has found its way into a sensor naturally. It is mainly because it is exceedingly sensitive to temperature variation. A pyroelectric nanogenerator can be externally exposed to an Iot growth through an electric biasing founded on the PyNG reference. This can top desire to satisfy the current IOT users concerned by ensuring output Pyroelectric nanogenerators has mandatory IOT sensor growth in line with electric compatibility. The excluded energy can be suitably utilized in maximum energy influencing other harvesting methods. This includes piezoelectric or triboelectric generators that align with energy content. Piezoelectric nanogenerators as well as triboelectric nanogenerators relies on energy rectification from natural heat, mechanical noises and machine to produce thermal power.Pyroelectric effect Pyroelectric devices, e.g., heat sensors, IR sensors, thermal imaging instruments and even fire alarm units and gas analyzers have been widely used after the discovery of pyroelectric effect (Rosen & Bulucea, 2009:823; Trinh et al., 2014:679). Figure 1 (A): Various applications available in pyroelectric materials. More recently, the authors of the present review paper claim there is a renaissance in the PyNG area especially after being revisited as pyroelectric energy harvesting systems they became even more attractive and challenging. Standard PyNG device structure: consists of three layers, including patterned

top-metal layer for both a hot receiver and an electrode, middle pyroelectric (with changes in heat being transformed into electrical charges via poling), and the bottom-electrode layer (Fig. 1b). Due to their pedestrian structure, the performance enhancement of PyNGs is largely related to material design and structural optimization. For example, enlarging the thermoelectric conversion power output through raising microphone sensitivity to temperature operating barrier such as surface treating (surface polarity treatment), material production including improvement to pyroelectric coefficient and thermal expansion amount in polarization change. Thus, this review is intended to unveil the operating principle of PyNGs, specifically for polymer- and ceramic-based PyNGs.

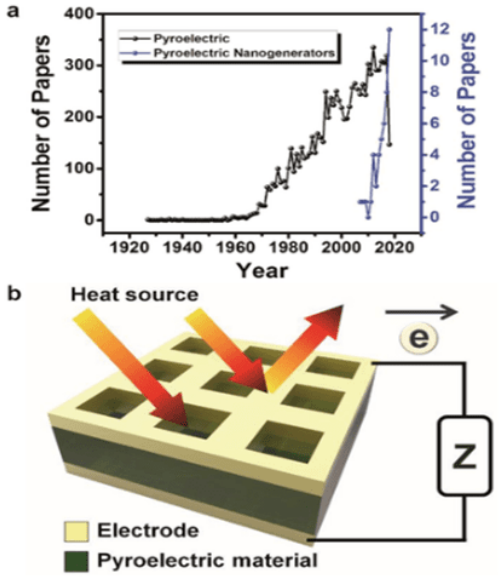

Figure 1. a) Time sequence of publications on pyroelectrics and pyroelectric nanogenerators in Scopus. b) Schematic illustration of a pyroelectric energy harvesting system.

2. MATERIALS AND METHODS

In this study and within the reviewed literature, various classes of materials have been employed for the fabrication of pyroelectric nanogenerators (PyNGs) and their hybrid systems:

1. **Polymer-Based Pyroelectric Materials**
   - **Polyvinylidene fluoride (PVDF):** a flexible ferroelectric polymer widely used in thin films and nanofibers due to its biocompatibility and ease of processing.
   - **Poly(vinylidene fluoride-co-trifluoroethylene) [P(VDF-TrFE)]:** exhibits enhanced β-phase crystallinity and higher pyroelectric coefficients compared to pure PVDF.
   - **Polyimide (PI):** used as an encapsulation material to provide thermal stability and insulation.
   - **Polydimethylsiloxane (PDMS):** applied as a substrate or encapsulant due to its high stretchability, flexibility, and low thermal conductivity, enabling strain-coupled PyNGs.
   - **Polyvinyl chloride (PVC):** employed as a protective encapsulation film to prevent oxidation and water-induced conductivity.
   - **Electrospun PVDF Nanofibers:** fabricated through electrospinning for wearable PyNGs with enhanced β-phase content.
   - **Erbium-doped PVDF (Er-PVDF):** developed to enhance polarization, β-phase formation, and infrared absorption.
2. **Ceramic-Based Pyroelectric Materials**
   - **Zinc oxide (ZnO):** utilized in nanowire arrays and thin-film structures, providing high pyroelectric coefficients and multifunctionality (e.g., self-powered sensors).
   - **Lead zirconate titanate (PZT):** a classical ferroelectric ceramic with high pyroelectric and piezoelectric coefficients.
   - **Barium titanate ($BaTiO_3$, BTO):** widely employed for its ferroelectric and pyroelectric behavior.
   - **Potassium niobate ($KNbO_3$) and $BiFeO_3$ (BFO):** alternative ferroelectric ceramics with strong thermal stability.

- **1,4-Diazabicyclo[2.2.2]octane perrhenate (dabcoHReO$_4$):** reported for its unique pyroelectric response.

3. **Electrode and Conductive Materials**
   - **Metals (Cu, Ag, Al):** used as electrodes and heat receivers.
   - **Silver nanowires (AgNWs):** provide transparent and flexible electrode layers.
   - **Indium tin oxide (ITO):** a transparent conducting oxide used for flexible and transparent PyNGs.
   - **Carbon nanotubes (CNTs):** integrated into polymer composites (e.g., PDMS-CNT) to enhance conductivity and stretchability.
   - **Graphene nanosheets:** employed as transparent, flexible, and high-thermal-conductivity electrodes.
   - **PEDOT:PSS with Polyvinylpyrrolidone (PVP):** conductive polymer networks enabling flexible, wearable devices.
4. **Encapsulation and Structural Materials**
   - **Polyurethane (TPU):** incorporated in nanofiber membranes for mechanical robustness.
   - **Liquid Crystal Display (LCD) films:** utilized for visualization of temperature gradients in hybrid systems.
   - **Surface-modified substrates (leaf-venation patterned PDMS, master-molded PDMS):** employed to improve thermal transfer and stretchability.

Overall, the combination of **flexible polymers, high-performance ferroelectric ceramics, and advanced conductive materials** enables the development of efficient PyNGs tailored for applications in self-powered IoT devices, wearable systems, and hybrid energy harvesting platforms.

3. RESULT

3.1. The Pyroelectric Effect

Pyroelectric materials inherently exhibit spontaneous polarization (Ps) in the absence of an electric field. The pyroelectric effect refers to the temporary variation in Ps caused by fluctuations in temperature (Ryu & Kim, 2021, p. 965). When temperature increases, thermal vibrations reduce Ps, thereby lowering the bound surface charges (Ryu & Kim, 2021, p. 966). Under open-circuit conditions, this generates an electrical potential, whereas under short-circuit conditions, an electric current flows through the external circuit (Cullen & Allwood, 2010, p. 2062).

The theoretical short-circuit current is expressed in **Equation (1)**, where i represents the generated current, Q is the pyroelectric charge, p is the pyroelectric coefficient, A denotes the surface area of the pyroelectric material, and t represents time. The unclamped pyroelectric coefficient under constant stress and electric field is further defined in **Equation (2)** (Shen et al., 2021, p. 968). Although the pyroelectric coefficient is fundamentally a vector quantity, it is often treated as scalar in experimental evaluations (Ryu & Kim, 2021, p. 969).

$$i = \frac{\mathrm{d}Q}{\mathrm{d}t} = pA\frac{\mathrm{d}T}{\mathrm{d}t} \quad (1)$$

$$p^{\sigma,E} = \left(\frac{\mathrm{d}P_s}{\mathrm{d}T}\right)_{\sigma,E} \quad (2)$$

To achieve accurate quantification, several static and dynamic evaluation methods have been proposed (POPESCU et al., 2013, p. 47). Static methods include charge compensation, hysteresis loop analysis, electrocaloric measurements, flat band-voltage shifts, X-ray photoelectron spectroscopy (XPS), and X-ray diffraction (XRD) coupled with density functional theory. Dynamic methods involve temperature ramping, optical techniques, periodic pulsing, laser modulation, and harmonic waveform analysis. While these methods provide precise insights into material properties, complex device designs and environmental factors often interfere with the actual performance of PyNGs. Hence, evaluating output current alongside physical parameters is considered a more practical approach. The pyroelectric coefficient of PyNGs is calculated using **Equation (3)**.

$$p = \frac{i}{A \cdot \mathrm{d}T/\mathrm{d}t} \quad (3)$$

As illustrated in **Figure 2a–c**, the working principle of PyNGs is based on temperature-driven changes in Ps (Zhang, 2020, p. 012001). For example, crystalline polymers with aligned molecular chains exhibit polarization due to covalent bond orientation, while ionic ceramic materials achieve polarization through asymmetric crystal structures (Li et al., 2014, p. 7762). In an ideal scenario, all dipoles would align in a uniform direction, but atomic vibrations disrupt this order. Under constant temperature, Ps and the dipole angle (θ) remain unchanged, resulting in no current flow (**Figure 2a**). When heated (dT/dt > 0), dipole orientations fluctuate around their axes due to thermal energy

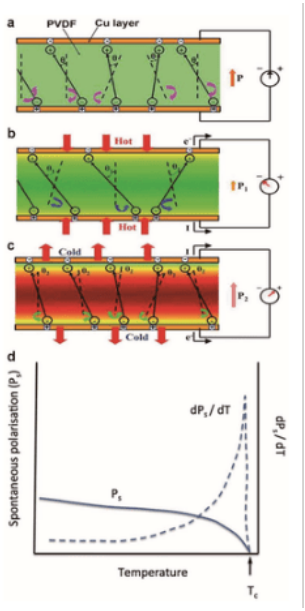

(**Figure 2b**).

Figure 2. a) Working principle of PyNG under constant temperature. b) Heated condition. c) Cooled condition. d) Relationship between temperature, Ps, and pyroelectric coefficientThe variation of spontaneous polarization (Ps) in pyroelectric materials with respect to temperature is illustrated in **Figure 2d** (Ryu & Kim, 2021, p. 5). As temperature increases, Ps decreases at different rates of polarization change. When the material reaches the Curie temperature (TC), Ps rapidly drops to zero, while the pyroelectric coefficient sharply rises. Although pyroelectric materials lose their pyroelectric properties above TC, strong polarization changes below TC can still be effectively utilized for pyroelectric energy harvesting. By controlling the operating temperature conditions, the pyroelectric coefficient of materials can be significantly enhanced, leading to a considerable increase in the output current of pyroelectric nanogenerators (PyNGs).

3.2 Polymer-Based Pyroelectric Nanogenerators

3.2.1. PyNGs Driven by Various Environmental Conditions

Ferroelectric materials such as **lead zirconate titanate (PZT)**, **barium titanate (BTO)**, **polyvinylidene fluoride (PVDF)**, and **poly(vinylidene fluoride-co-trifluoroethylene) [P(VDF-TrFE)]** exhibit spontaneous polarization, thereby possessing both pyroelectric and piezoelectric properties. These materials have been widely applied in IR sensors, actuators, and energy harvesters (Zhang, 2020, p. 3). Among them, polymer-based PyNGs primarily utilize ferroelectric polymers such as PVDF and P(VDF-TrFE). Although PVDF has a relatively low pyroelectric coefficient, it offers high mechanical flexibility and biocompatibility, making it suitable for wearable devices (Ryu & Kim, 2021, p. 7).

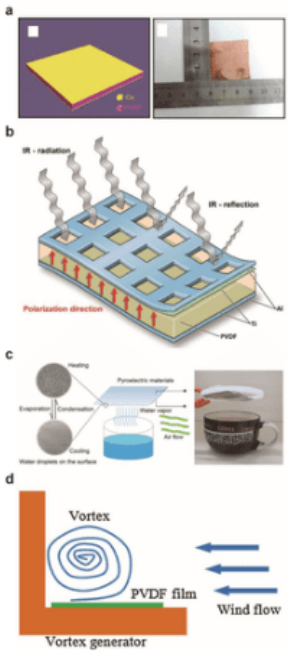

Figure 3. Illustrates various thin-film polymer-based PyNGs. (a) Schematic and real images of a PVDF thin film-based PyNG (Leng et al., 2014, p. 47). (b) Schematic representation of an IR-radiation-driven PyNG (Zabek et al., 2015, p. 48). (c) Schematic and real images of a water-vapor-powered PyNG (Gao et al., 2016, p. 50). (d) Schematic representation of a wind-driven PVDF-based PyNG (Raouadi & Touayar, 2016, p. 51).Leng et al. developed a high-performance PVDF-based PyNG with a simple **Cu/PVDF/Cu** structure, employing hot and cold water as thermal energy sources (**Figure 3a**) (Murehwa et al., 2012, p. 22). To prevent oxidation and water-induced conductivity, a **30 µm thick polyvinyl chloride (PVC) thin film** encapsulated the device. The PyNG was tested using alternating hot flows (40, 60, 80 °C) and cold flows (0 °C). As the hot flow temperature increased, the device's output rose from **6 to 11 µA**. Moreover, by mechanically deforming the PyNG under varying temperatures, the output voltage dramatically increased to **100–190 V**, while the maximum output power reached **126 µW** under optimal load resistance. Finite element method (FEM) simulations confirmed that the PVDF film exhibited a pyroelectric coefficient of **2.7 nC cm−2 K−1**, with simulated electrical potential distributions peaking at **774 V**. In practical demonstrations, the PyNG successfully powered **42 LEDs** and charged a **100 µF capacitor**.Zabek et al. presented a flexible PVDF-based PyNG featuring a **micropatterned top electrode layer** to enhance heat transfer and temperature fluctuations (**Figure 3b**) (Trinh et al., 2014, p. 678). By exposing partially covered aluminum electrodes to **IR radiation**, they achieved larger temperature variations, especially in devices with **45–53% electrode coverage**, resulting in **400% higher voltage and current outputs**. This highlights the importance of balanced electrode design for maximizing energy conversion efficiency.Gao et al. fabricated large flexible P(VDF-TrFE) PyNGs driven by **hot water vapor**, leveraging rapid temperature oscillations (**Figure 3c**) (Li et al., 2014, p. 7762). Encapsulated with **polyimide (PI) tape**, the device experienced rapid heating up to **65 °C** and cooling down to **40 °C** through alternating condensation and evaporation cycles. This process yielded a peak voltage of **160 V**, a peak current of **5.5 µA**, and a maximum power output of **220 µW**, which successfully powered a **digital watch, LEDs, and a capacitor**.Raouadi and Touayar explored **wind-driven PyNGs** using a **vortex generator** to induce turbulence and enhance convective heat transfer (**Figure 3d**) (Soto & Vergara, 2014, p. 110). Their PVDF-based device achieved a maximum output power of **2.8 µW cm−2** under optimal load resistance, sufficient to operate a **white LED** and a **sound buzzer**.

3.2.2. Development of Pyroelectric Materials

Polymer-based PyNGs are widely utilized to harvest thermal energy under diverse environmental conditions due to their flexibility and thin-film configurations. However, their relatively low pyroelectric coefficients limit overall performance. To address this challenge, various strategies have been proposed, including crystallinity enhancement, strain coupling effects, and polymer modification (Cullen & Allwood, 2010, p. 2062).

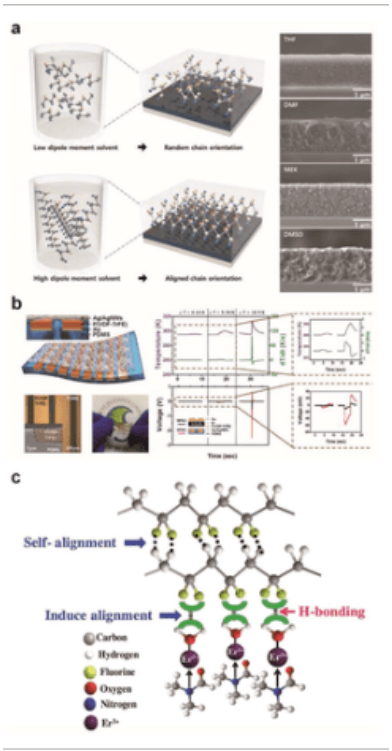

Figure 4. Presents strategies for improving the output power of PyNGs. (a) Schematic images showing the difference between low- and high-crystalline P(VDF-TrFE) (Kim et al., 2017, p. 52). (b) Schematic illustrations of a stretchable PyNG and its enhanced output performance (Lee et al., 2015, p. 55). (c) Schematic diagram of the β-phase nucleation process in Er-PVDF films (Ghosh et al., 2017, p. 60).Kim et al. demonstrated that solvents with high dipole moments significantly improved the crystallinity of P(VDF-TrFE), thereby enhancing its pyroelectric coefficient (**Figure 4a**) (Maglogianni et al., 2023, p. 104995). Solvents such as tetrahydrofuran (THF), methylethyl ketone (MEK), dimethylformamide (DMF), and dimethylsulfoxide (DMSO), with dipole moments of 1.75, 2.7, 3.8, and 4.1 D respectively, were used to dissolve P(VDF-TrFE). Characterization via X-ray diffraction (XRD) and differential scanning calorimetry (DSC) revealed that films processed with higher dipole moment solvents exhibited superior crystallinity. Gel permeation chromatography (GPC) confirmed the correlation with longer chain lengths and higher molecular weight. As a result, highly crystalline P(VDF-TrFE) films displayed stronger dipole alignment, yielding a 1.4-fold increase in both peak voltage and current compared to low-crystalline films. Thus, solvent engineering represents a promising pathway for improving pyroelectric material efficiency.Lee et al. advanced the concept of stretchable PyNGs by exploiting strain coupling between P(VDF-TrFE) and polydimethylsiloxane (PDMS) substrates (**Figure 4b**) (Virili et al., 2015, p. 28). PDMS, possessing a higher thermal expansion coefficient than P(VDF-TrFE), induced compressive stress upon heating, thereby altering internal polarity and amplifying pyroelectric output. Spectroscopic analysis using Fourier transform infrared (FT-IR) and XRD confirmed the β-phase formation in the patterned films. The strain-coupled devices achieved up to fivefold improvement in pyroelectric output under identical thermal conditions. Furthermore, due to PDMS's low thermal conductivity, greater heat retention occurred within P(VDF-TrFE), reinforcing the strain-induced polarization effect. The stretchable PyNG demonstrated mechanical robustness with up to 15% elongation without loss of performance, successfully powering multiple LEDs and liquid crystal displays (LCDs).Ghosh et al. reported the development of Er^{3+}-modified PVDF (Er-PVDF) films, which exhibited enhanced pyroelectric properties owing to the formation of a self-polarized ferroelectric β-phase and porous structures (**Figure 4c**) (Zhang et al., 2025, p. 124610). The incorporation of Er^{3+} ions promoted rapid crystallization, resulting in flower-like surface morphologies that improved flexibility while simultaneously boosting thermal stability. X-ray photoelectron spectroscopy (XPS) confirmed the successful doping of Er^{3+} within the PVDF matrix. The enhanced optical activity of Er^{3+} ions increased infrared (IR) absorption, enabling efficient conversion of small-scale thermal fluctuations into electrical energy. The Er-PVDF PyNG generated a peak current of 13 nA under a low heating rate (<1 K s−1), sufficient to charge a 4.7 μF capacitor and operate low-power electronic devices. These findings highlight rare-earth ion modification as a viable approach for advancing pyroelectric materials.

3.2.3. Wearable Pyroelectric Nanogenerators

The human body represents a readily available thermal energy source, making pyroelectric nanogenerators (PyNGs) particularly suitable for powering wearable electronic devices. To integrate PyNGs into wearable applications, the use of materials that possess **flexibility, stretchability, or fiber-like structures** is essential. Xue et al. developed a system combining an N95 respirator with a PVDF thin-film PyNG to harvest energy from human respiration (Figure 5a) (Ryu & Kim, 2021, p. 4). Their work demonstrated a **self-powered breathing sensor** in which a flexible PVDF film was attached to a conventional respirator, enabling sustainable energy harvesting and real-time respiration monitoring. The PVDF thin film, measuring 3.5 cm × 3.5 cm with a thickness of 30 μm, was directly exposed to exhaled air at body temperature. The device recorded a temperature variation rate of 13 °C s^{-1}, generating a peak output of 2.5 μA and 42 V. Under a load resistance of 50 MΩ, the maximum power output reached 8.31 μW, with stable performance sustained for ten days without noticeable degradation. Notably, condensation of water vapor from exhaled air accelerated heating but slowed cooling, thereby influencing the PyNG's response. To validate its energy storage capability, a simple circuit consisting of a 10 μF capacitor and a rectifier was employed, successfully charging the capacitor to 1 V in 18 seconds and powering LEDs and an LCD (Ryu & Kim, 2021, p. 6).

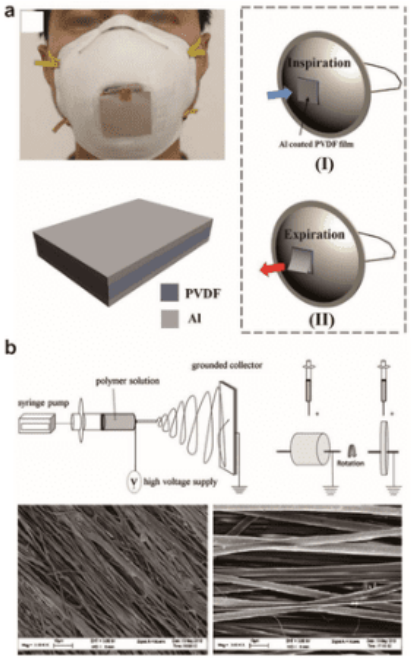

Figure 5. Wearable PyNGs based on polymer materials. (a) Real photograph and schematic illustration of a wearable PyNG. Reproduced with permission (Copyright 2017, Elsevier Ltd). (b) Schematic of the electrospinning process and SEM image of fibrous PVDF. Reproduced with permission (Copyright Taylor & Francis).Although PVDF thin films are promising, their limited flexibility and stretchability hinder wearable applications. To address this, Mokhtari et al. employed an **electrospinning process** to fabricate PVDF nanofibers (Figure 5b). Electrospinning under low chamber temperatures or conditions favoring rapid solvent evaporation facilitated the formation of the β-ferroelectric phase without requiring post-treatment. Conversely, mechanical stretching induced by rotational force was found ineffective in stabilizing the β phase. The process involved applying a high voltage to eject PVDF solution at a controlled flow rate, where electrostatic forces overcame the liquid's surface tension. The charged jet was then collected on a grounded plate, during which solvent evaporation allowed β-phase PVDF nanofibers to be deposited. The **tip-to-collector distance** played a critical role in determining the nanofiber diameter. Analytical methods such as FT-IR, XRD, and DSC confirmed the presence of the β phase, validating that electrospinning could yield β-phase PVDF fibers suitable for wearable energy harvesting applications without additional poling (Zhang, 2020, p. 112).

3.2.4. Stretchable Hybrid Pyroelectric Nanogenerators

To achieve **highly stretchable PyNGs** for wearable electronics, Lee et al. designed a hybrid system integrating patterned PDMS-carbon nanotube (CNT) composites with graphene nanosheets (Figure 6). Graphene, characterized by superior thermal conductivity and mechanical flexibility, replaced conventional metal electrodes (Li et al., 2014,

p. 7761). The fabrication process involved forming a patterned PDMS-CNT substrate using a silicon master mold, followed by spin-coating P(VDF-TrFE) directly onto the micropatterned surface. The sample was subsequently annealed at 140 °C for two hours, and XRD and FT-IR analyses confirmed the β-ferroelectric phase. A multilayer graphene sheet was then transferred to the P(VDF-TrFE), ensuring conformity to the PDMS-CNT patterns and enhancing stretchability compared to flat configurations (Ryu & Kim, 2021, p. 8).The hybrid PyNG leveraged both **piezoelectric and pyroelectric effects**. Mechanical deformation altered polarization via the piezoelectric effect, while thermal fluctuations induced polarization changes through the pyroelectric effect. When subjected to synchronized deformation and temperature change, internal polarization shifts were amplified. For instance, releasing and heating enhanced polarization change, while compression combined with heating produced a similar reinforcing effect. The device exhibited a piezoelectric output of 1 V, a pyroelectric output of 0.4 V, and a combined output of 1.4 V under simultaneous stimulation. Long-term testing showed stable performance under 30% stretching, indicating the reliability of patterned substrates in enhancing device stretchability for wearable use (Cullen & Allwood, 2010, p. 2063).

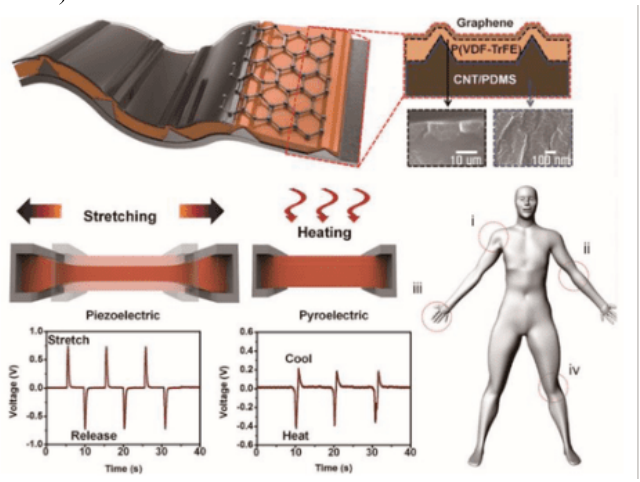

Figure 6. Schematic illustration of a highly stretchable hybrid PyNG. Reproduced with permission (Copyright 2013, WILEY-VCH Verlag GmbH & Co. KGaA).

3.2.5 Hybrid Pyroelectric Nanogenerators

The integration of multiple energy harvesting mechanisms has emerged as an effective strategy to improve the overall energy conversion efficiency of nanogenerators. Consequently, hybrid devices that combine pyroelectric, piezoelectric, triboelectric, and photovoltaic energy harvesting mechanisms have been developed to achieve superior performance. In designing hybridized systems, impedance matching among different energy harvesters plays a critical role. When the individual harvesters possess similar impedance, no special electrical circuitry is required. However, for harvesters with different impedance values, auxiliary components such as capacitors, batteries, or dedicated power management circuits are necessary to coordinate the output effectively (Rosen & Bulucea, 2009, p. 823).A representative example was presented by **Ryu & Kim.**, who developed a piezoelectric–pyroelectric hybrid nanogenerator (PPNG) based on polyvinylidene fluoride (PVDF) nanofiber membranes (NFMs), as shown in **Figure 7**. The device was fabricated through an electrospinning process using thermoplastic polyurethane (TPU), carbon nanotube slurry (CNTS), PVDF, and PEDOT:PSS–polyvinyl pyrrolidone (PVP) conductive NFMs (CNFM). The fabricated NFMs exhibited distinct morphologies confirmed by scanning electron microscopy (SEM) and X-ray diffraction (XRD). The electrical conductivity of the CNTs layer was ~4.4 × 10−3 S cm−1, while the CNFM conductivity was ~1.27 × 10−4 S cm−1. Due to the flexibility imparted by electrospun electrodes, the hybrid nanogenerator was suitable for wearable systems. With an effective device size of 4 × 4 cm², it generated 2.85 μJ under a 3 Hz impact–release cycle. The piezoelectric contribution increased with both force and speed of impact, while the pyroelectric component produced ~20 nA under small temperature fluctuations. The coupling of piezoelectric and pyroelectric responses resulted in a synergistic enhancement in spontaneous polarization, enabling the device to power wearable systems such as walking-based and arm-bending energy harvesters (Ryu & Kim, 2021, p. 4).

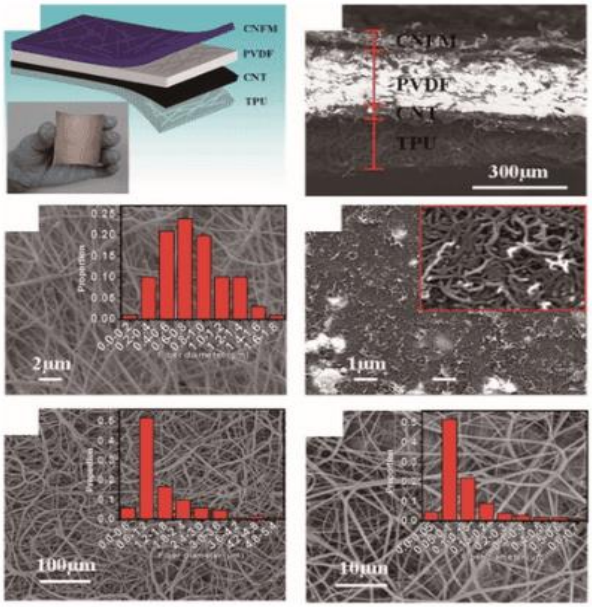

Figure 7. Nanowire ferroelectric polymer-based PyNG (Reproduced with permission, Copyright 2018, The Royal Society of Chemistry).

Another noteworthy demonstration was reported by **Zhang et al.**, who fabricated a flexible, transparent, and biocompatible hybrid nanogenerator integrating triboelectric, piezoelectric, and pyroelectric mechanisms (**Figure 8a**). The device was composed of polydimethylsiloxane (PDMS), PVDF, and silver nanowires, achieving 82% optical transmission due to the high transparency of its components. A replicated leaf-venation (LV) pattern mold was employed to enhance electrode conductivity. Mechanical energy was harvested through finger pressing, which generated surface triboelectric charges on PDMS and induced dipole polarization in PVDF, resulting in 55 V output. Additionally, the pyroelectric response contributed 86 V under temperature variations. Beyond power generation, this hybrid system demonstrated promising applications as flexible wearable sensors for detecting heartbeat, swallowing, neck tilting, and coughing. Furthermore, the incorporation of a liquid-crystal display (LCD) film between electrodes enabled visual representation of temperature gradients by color changes (Zhang et al., 2025, p. 124611).

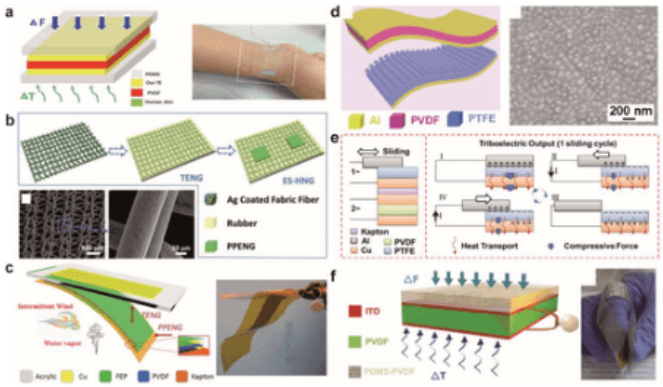

Figure 8. Mechanical and thermal hybrid NGs: a) schematic and real photo image of hybrid NG; b) tribo/piezo/pyroelectric hybrid NG; c) flexible and thin hybrid NG; d) patterned PVDF-based hybrid NG; e) sliding heat-induced hybrid NG; f) one-structure-based hybrid NG.

Similarly, **Cullen & Allwood** designed a tribo–piezo–pyroelectric hybrid nanogenerator with additional functionality as an electromagnetic shielding device (**Figure 8b**). The system was fabricated using PVDF, Ag, and rubber composites. Reducing electromagnetic radiation exposure is a growing concern due to its potential health risks (Cullen & Allwood, 2010, p. 2062). Their stretchable hybrid NG (ES-HNG) combined a conductive anti-radiation fabric with rubber, achieving 40% stretchability. Mechanical deformation induced triboelectric and piezoelectric outputs, while thermal changes generated pyroelectric responses. The device produced peak currents of

6 nA (under 0.3 N force), 18 nA (under bending), and 15 nA (under temperature variation). It successfully harvested biomechanical energy to charge capacitors, reduced electromagnetic radiation from 6261 to 0 μW cm−2, and demonstrated protective applications for pregnant women (Maglogianni et al., 2023, p. 7).

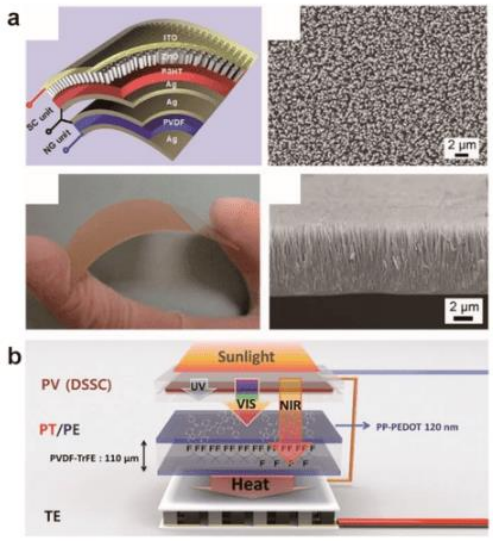

Figure 9. Solar, mechanical, and thermal hybrid nanogenerators (NGs). (a) Schematic illustration of a ZnO nanowire and PVDF-based solar–thermal hybrid NG. Reproduced with permission, Copyright 2012, American Chemical Society. (b) Schematic illustration of a P(VDF-TrFE)-based hybrid NG integrated with a dye-sensitized solar cell (DSSC) and thermoelectric device. Reproduced with permission, Copyright 2015, American Chemical Society.Further advancements included wind-thermal hybridization (**Figure 8c**) by **Jiménez-Arreola et al.**, and surface-modified PVDF-based devices for cathodic protection applications (**Figure 8d**) by **Jiménez-Arreola et al.**. In another significant study, **Zi et al.** demonstrated a triboelectric–piezoelectric–pyroelectric hybrid system that converted both mechanical sliding/pressing and frictional heat into electricity (**Figure 8e**). This system achieved peak outputs of 1132 V and 1.45 mA m−2 from the triboelectric component, with additional contributions from pyroelectric and piezoelectric mechanisms, enabling LED operation and capacitor charging (Jiménez-Arreola et al., 2018, p. 579).Large-scale transparent devices were also developed by **Li et al.**, who fabricated a one-structure hybrid nanogenerator using PVDF nanowires, PDMS, and indium tin oxide (ITO) electrodes (**Figure 8f**). With a transparency exceeding 95%, the device achieved peak outputs of 20 μA (TENG/PENG) and 120 V (PyNG), successfully powering light bulbs and capacitors. This confirmed the practicality of flexible polymer-based transparent NGs for wearable energy harvesting (Li et al., 2014, p. 7761).In efforts to further boost performance, integration of solar cells with hybrid nanogenerators was explored. **Zhang** combined a PVDF-based pyroelectric–piezoelectric NG with a ZnO nanowire/poly(3-hexylthiophene) (P3HT) heterojunction solar cell (**Figure 9a**). Under simultaneous solar and thermal excitation, the hybrid device exhibited improved output, successfully charging a Li-ion battery to operate LEDs (Zhang, 2020, p. 6). Likewise, **Popescu et al.** introduced a multifunctional system combining pyroelectric, thermoelectric, and dye-sensitized solar cell (DSSC) components (**Figure 9b**). By incorporating PEDOT-coated P(VDF-TrFE) films, the device achieved a 22 μW m−2 pyroelectric output under NIR irradiation and 11.7% hybridized energy conversion efficiency, surpassing standalone DSSCs (Popescu et al., 2013, p. 4).Overall, the hybridization of pyroelectric nanogenerators with complementary energy harvesting systems demonstrates significant potential in enhancing power density, functional versatility, and practical applications. Nevertheless, continued improvements in pyroelectric coefficients and device integration remain essential for achieving higher conversion efficiencies and simplified device architectures.

3.3 Ceramic-Based Pyroelectric Nanogenerators

3.3.1. ZnO-Based Pyroelectric Nanogenerators

Ceramic pyroelectric materials, including ZnO, PZT, $KNbO_3$, 1,4-diazabicyclo[2.2.2]octane perrhenate (dabcoHReO4), $BiFeO_3$ (BFO), and $BaTiO_3$ (BTO), exhibit higher pyroelectric coefficients and stronger resistance to thermal shocks compared to polymer-based pyroelectric materials discussed earlier. Consequently, ceramic-based pyroelectric nanogenerators (PyNGs) are widely applied in high-resolution thermal sensing systems (Ryu & Kim, 2021, p. 5).

Yang et al. developed a ZnO nanowire-array PyNG (Figure 10a), where vertically aligned ZnO nanowires were synthesized on an ITO substrate with an Ag electrode deposited on top to establish a Schottky contact (Yang, 2012, p. 88). Temperature fluctuations induced anisotropic polarization within the ZnO nanowires, leading to charge displacement and electron flow through an external circuit (Shen et al., 2021, p. 968). Current–voltage (I–V) characterization confirmed the Schottky junction between ZnO and Ag. Under a thermal variation rate of 0.5 $K \cdot s^{-1}$, the device produced a maximum output of 5.8 mV and 108 pA. Notably, the pyroelectric coefficient of the ZnO nanowires (1.2–1.5 $nC \cdot cm^{-2} \cdot K^{-1}$) was significantly higher than earlier reports due to the c-axis orientation of the nanowire arrays (Li et al., 2014, p. 7762). COMSOL multiphysics simulations of a single ZnO nanowire revealed a potential distribution between −3.1 and 2.6 V, exceeding the experimental data due to charge-carrier screening effects (Zhang, 2020, p. 7).

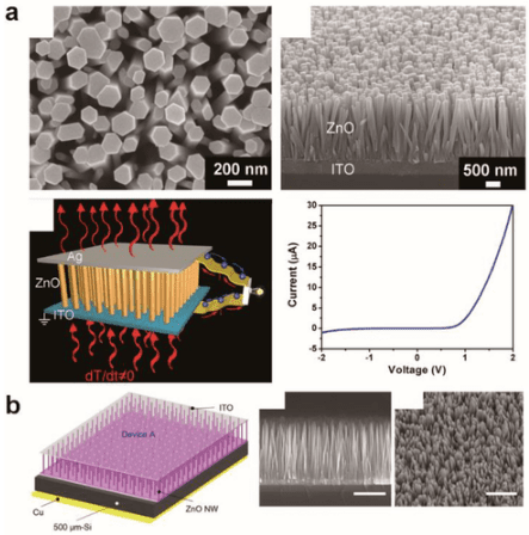

Figure 10. ZnO-based PyNGs. (a) SEM and schematic of the ZnO-based PyNG. Reproduced with permission (Yang, 2012). (b) Schematic of a ZnO-based PyNG integrated with a self-powered photodetector. Reproduced with permission (Wang, 2017).Later, Wang et al. reported a flexible PyNG utilizing wurtzite ZnO nanowires that functioned both as a pyroelectric generator and as a self-powered photosensor (Figure 10b) (Wang, 2017, p. 99). The intrinsic pyroelectric potential of ZnO nanowires modulated charge transport across the Si/ZnO p–n junction, dynamically altering the depletion region during near-infrared (NIR) irradiation. This interaction enabled photodetection without external bias. During NIR exposure, the pyroelectric potential widened the depletion region, inducing electron flow, whereas switching off irradiation reversed the potential, narrowing the depletion zone and driving a reverse current. The PyNG generated peak currents of 2 μA under moderate NIR exposure, which increased to 1 mA under intense irradiation, achieving an on/off photocurrent ratio of up to 10^7 (Rosen & Bulucea, 2009, p. 823).

3.3.2. PZT-Based Pyroelectric Nanogenerators

Yang et al. also investigated PZT-film PyNGs, leveraging their intrinsically high pyroelectric coefficients for energy harvesting and self-powered nanosystems (Figure 11a) (Yang, 2012, p. 100). A 175 μm thick PZT layer was deposited on a 300 nm nickel substrate with a Ni top electrode. Under a thermal fluctuation rate of 0.2 $K \cdot s^{-1}$, the device produced 2.8 V and 42 nA, with a calculated pyroelectric coefficient of 80 $nC \cdot cm^{-2} \cdot K^{-1}$—far exceeding ZnO counterparts (Maglogianni et al., 2023, p. 104995). At higher thermal rates, the PyNG generated 22 V, 430 nA, and a peak power density of 0.2 $mW \cdot cm^{-3}$. Furthermore, the PyNG demonstrated long-term stability, sustaining output for over 60 s, which was 30 times greater than previously reported piezoelectric nanogenerators (Cullen & Allwood, 2010, p. 2063). Practical feasibility was validated by charging a Li-ion battery from 650 to 810 mV within 3 hours, storing 23 nAh of energy.

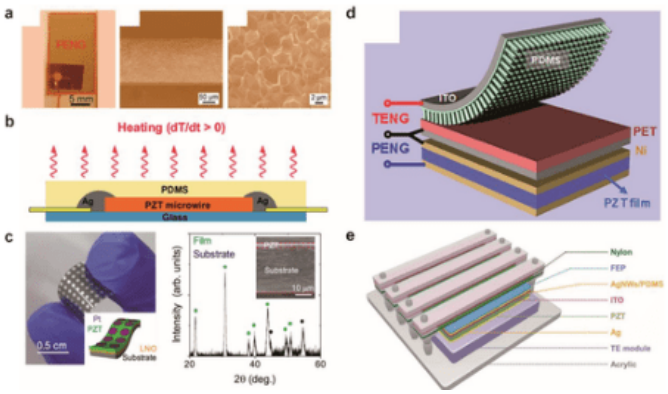

Figure 11. PZT-based PyNGs. (a) SEM and photo of PZT film PyNG (Yang, 2012). (b) Schematic of single PZT microwire PyNG (Yang, 2012). (c) Hybrid PZT-based PENG–PyNG on flexible substrate (Ko, 2016). (d) PZT–PDMS hybrid PyNG/TENG for self-powered degradation applications (Yang, 2013). (e) Integrated piezo–tribo–pyro–photoelectric hybrid NG (Zhang, 2016).Further advances included PZT micro/nanowire PyNGs for thermal sensing, where fingertip temperature variations were successfully detected (Figure 11b) (Yang, 2012, p. 102). Devices demonstrated rapid response (0.9 s) and decay times (3 s), with linear voltage–temperature correlation, suitable for calibration in thermal sensing.Hybrid flexible PyNG–PENG devices were also demonstrated (Figure 11c), showing robust operation under high humidity (70% RH) and alkaline conditions (pH 13), maintaining performance under ultraviolet exposure (Ko, 2016, p. 103). Other studies reported hybrid TENG–PyNG systems for electrocatalytic oxidation of pollutants (Figure 11d), where harvested energy drove electrodegradation of methyl orange in solution (Yang, 2013, p. 106).Finally, Zhang et al. introduced a multifunctional integrated device (Figure 11e), combining pyroelectric, piezoelectric, triboelectric, and photovoltaic elements into a single structure (Zhang, 2016, p. 107). This multimodal NG achieved peak PyNG output of 100 V and 480 nA, and in practical application, successfully charged a 10 μF capacitor to 5.1 V within 90 s, illustrating the potential of multifunctional nanogenerators for autonomous energy harvesting (Trinh et al., 2014, p. 681).

3.3.3 Lead-Free Ceramic-Based Pyroelectric Nanogenerators

For wearable PyNG applications, the **non-toxic nature** of pyroelectric materials is essential to ensure biocompatibility. Although PZT-based PyNGs exhibit high energy-conversion efficiency, the development of **lead-free alternatives** is inevitable for safe and sustainable applications.Yang et al. reported a **single-crystalline lead-free $KNbO_3$ nanowire PyNG** (Figure 12) (Yang, 2012, p. 89). The nanowires were synthesized via a hydrothermal method and embedded in PDMS with a volume ratio of 7:3 to impart mechanical flexibility. The composite film was spin-coated on an ITO substrate, with Ag serving as the top electrode. Transmission electron microscopy (TEM) and selected area electron diffraction (SAED) confirmed the perovskite phase structure, with the nanowire growth direction along [011]. High-resolution TEM further verified crystallinity, while SEM images showed uniform dispersion of nanowires in PDMS without aggregation. The PyNG achieved a peak output of **10 mV and 120 pA** at a thermal fluctuation rate of 2 $K \cdot s^{-1}$. Although PDMS reduced volumetric efficiency, it enabled **mechanical flexibility**, a key factor for practical wearable devices.

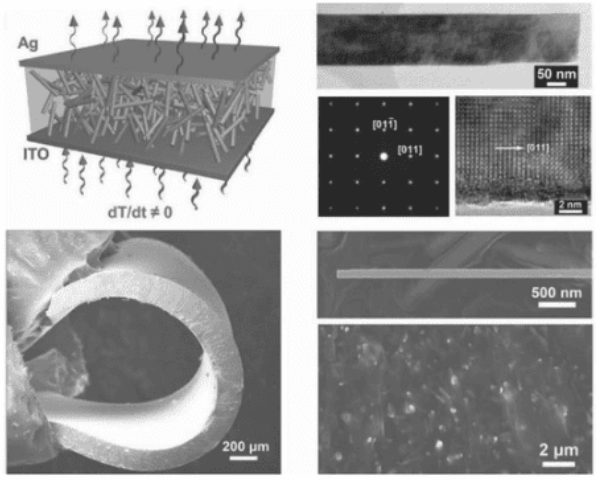

Figure 12. Schematic diagram of $KNbO_3$-based PyNG and TEM/SEM analysis of $KNbO_3$–PDMS composite film. Reproduced with permission (Yang, 2012). Copyright 2012, WILEY-VCH Verlag GmbH & Co. KGaA, Weinheim.

Another lead-free candidate was **dabcoHReO₄ nanofibers**, introduced by Isakov et al. (Figure 13) (Isakov, 2014, p. 108). The fibers were fabricated by electrospinning, and XRD confirmed crystalline orientation with dominant Bragg reflections at (200) and (110). Raman spectra further validated the single-crystal alignment, indicating consistent polarization direction. Piezoresponse force microscopy (PFM) revealed a well-defined hysteresis loop with a piezoelectric coefficient of 20 $pm \cdot V^{-1}$. The device generated a peak current of **200 pA** under a thermal fluctuation of 0.2 $K \cdot s^{-1}$, with a calculated pyroelectric coefficient of **8.5 $\mu C \cdot m^{-2} \cdot K^{-1}$**. Although lower than bulk dabcoHReO₄, the fiber mat structure facilitated integration into **flexible and wearable electronics**.

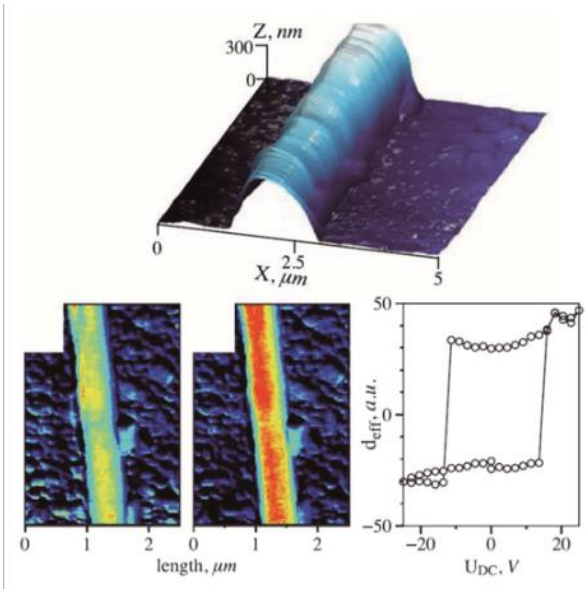

Figure 13. Surface morphology and PFM analysis of dabcoHReO₄ nanofiber-based PyNG. Reproduced with permission (Isakov, 2014). Copyright 2014, AIP Publishing LLC.

Ji et al. demonstrated a **$BaTiO_3$ (BTO)-based hybrid NG** combining piezoelectric, pyroelectric, triboelectric, and photoelectric properties (Figure 14) (Ji, 2017, p. 109). A BTO ceramic disk was fabricated by dry pressing, then coated with PDMS as a protective layer. A fluorinated ethylene propylene (FEP) film was added as a triboelectric component, with nylon/acrylic used as the counter-material. A commercial thermoelectric module was also integrated for thermal harvesting. XRD confirmed the tetragonal ferroelectric phase of BTO. The PyNG achieved a peak output of **1.5 V and 15 nA**, while the solar cell contributed **40.5 nA at 0.8 V** (average 10 nA at 0.6 V). The TENG–PENG hybrid device produced **3.5 µA**, although voltage was negligible (<0.1 V). The hybrid NG exhibited a pyroelectric coefficient of **26 $nC \cdot cm^{-2} \cdot K^{-1}$**, and the coupling of pyroelectric and photovoltaic effects enhanced current output by **86%** under simultaneous thermal and light excitation. Practical demonstration included charging a **0.33 µF capacitor to 1.1 V within 10 s**.

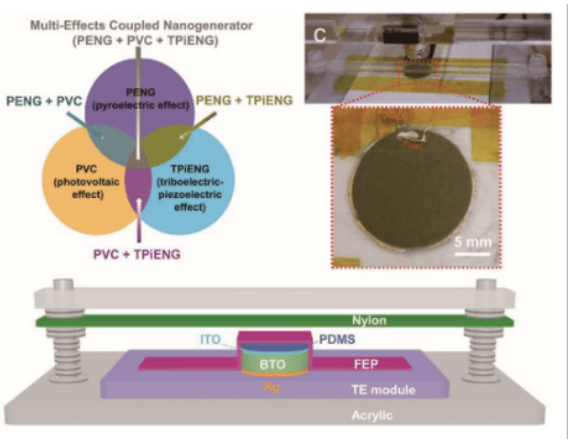

Figure 14. Schematic and real images of the BTO-based hybrid NG. Reproduced with permission (Ji, 2017). Copyright 2017, WILEY-VCH Verlag GmbH & Co. KGaA, Weinheim.

Qi et al. developed a **$BiFeO_3$ (BFO)-based hybrid NG** exploiting photovoltaic–pyroelectric coupling for self-powered photodetection (Figure 15) (Qi, 2017, p. 110). Hydrothermally synthesized BFO powders exhibited a perovskite phase as confirmed by XRD. The device architecture (ITO/BFO/Ag) formed Schottky barriers at both interfaces. Under a temperature change rate of 0.2 $K \cdot s^{-1}$ and 450 nm illumination, the hybrid NG generated **0.13 V and 8.8 nA**, while the photovoltaic contribution was only 2 nA. Due to different load resistances for PyNG and solar cell, the hybrid NG exhibited dual resistance matching. Remarkably, the hybrid NG displayed a responsivity nearly **978% higher** than conventional solar cells and a rapid recovery time of 0.8 s after light irradiation. A **3×3 photodetector array** was fabricated, enabling high-resolution real-time signal mapping on a BFO disk.

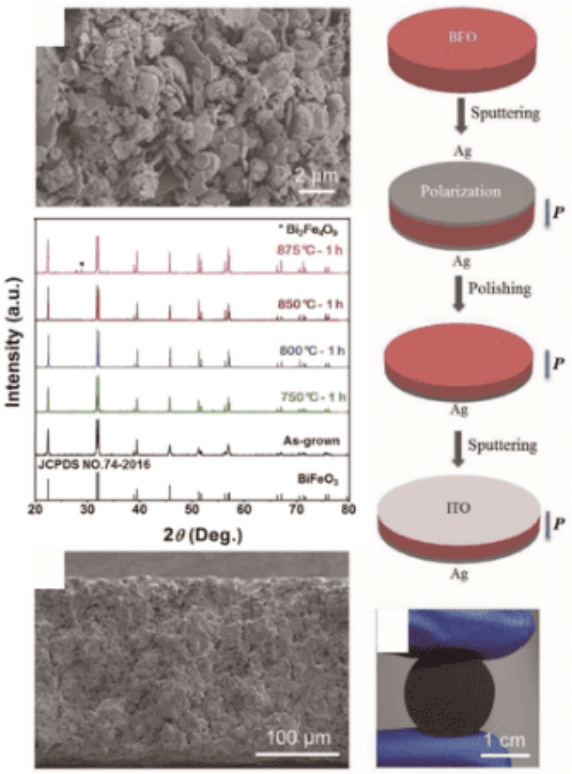

Figure 15. SEM and XRD analysis of BFO and schematic of BFO-based PyNG fabrication. Reproduced with permission (Qi, 2017). Copyright 2017, WILEY-VCH Verlag GmbH & Co. KGaA, Weinheim.

Overall, these studies highlight the **promising role of lead-free pyroelectric materials ($KNbO_3$, dabcoHReO$_4$, BTO, BFO)** as safer alternatives to PZT, enabling flexible, multifunctional, and environmentally benign PyNGs for wearable and optoelectronic applications.

3.4 Other Applications of Pyroelectric Nanogenerators (PyNGs)

Future development of PyNGs requires both **innovative applications** and **enhancement of pyroelectric coefficients**. One promising approach is the **thermal nanophotonic–pyroelectric (TNPh–pyro) coupling effect**, which can overcome the limitations of restricted thermal fluctuations in conventional PyNGs (Wang, 2017, p. 111).

Wang et al. designed a TNPh–pyro device that utilized a **nanophotonic structure** to enhance pyroelectric performance while maintaining high optical transparency (Figure 16). The structure consisted of periodically layered TiO_2 and mesoporous SiO_2, capped with mesoporous TiO_2/Cu. A **PVDF film** served as the pyroelectric layer, functioning as an outdoor solar heat harvester. The TNPh stack selectively reflected **near-infrared (NIR)** light, absorbed UV, and transmitted visible light, enabling **simultaneous thermal harvesting, cooling, air purification, and natural lighting** (Wang, 2017, p. 113).Structural characterization using XRD confirmed the crystal phases of TiO_2 and SiO_2. Optical measurements showed that the TNPh–pyro device transmitted 69.5% of visible light and 35% of NIR, fulfilling typical transparency standards for architectural windows. Under simulated solar irradiation (100 $mW \cdot cm^{-2}$), bare glass reached 33.1 °C, while the TNPh–pyro device remained at 29 °C, yielding **up to 45% cooling energy savings** (Wang, 2017, p. 115).

Beyond passive cooling, UV irradiation of the TiO_2/Cu film facilitated the decomposition of ethanol, isopropanol, and formaldehyde vapors, providing an additional **air-purification function**. Pyroelectric harvesting performance was also improved: the TNPh–pyro device generated **8.2 V and 23.5 nA**, representing a ~50% enhancement compared with pristine PVDF. In a practical demonstration, a **TNPh–pyro-roofed house** maintained an internal temperature **4.2 °C lower** than a glass-roofed house, while generating a peak output of **32 V and 126 nA**.These findings illustrate that coupling **nanophotonic thermal management with pyroelectric energy harvesting** can significantly improve both performance and multifunctionality. However, further progress also requires **material-level innovations**. Although controlling rapid thermal fluctuations can temporarily boost performance, the **pyroelectric coefficient** remains the most critical factor, as it is an intrinsic material property. Current discrepancies between theoretical and experimental results arise from imperfect crystal structures, defects, polarization instabilities, and thermal operating limits. Addressing these limitations through **heat transfer engineering, defect control, and structural optimization** will be key to advancing PyNG performance.

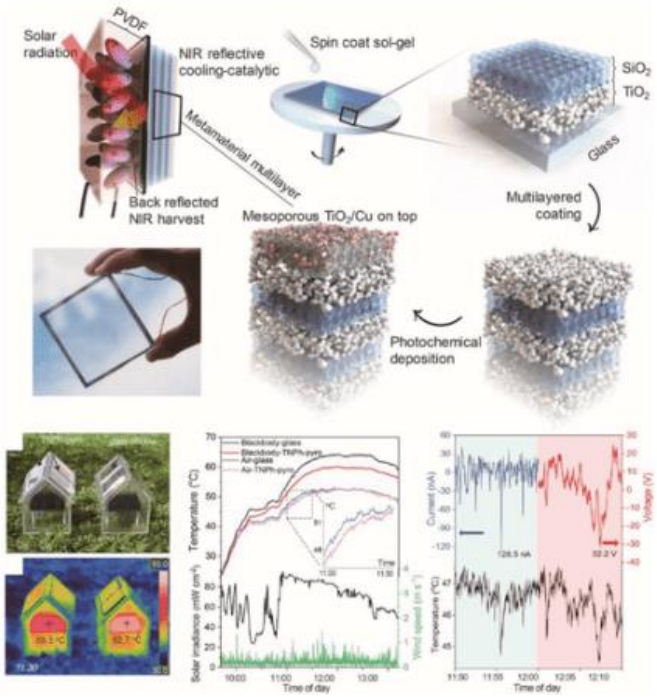

Figure 16. Schematic of TNPh–pyro fabrication process and application. Reproduced with permission (Wang, 2017). Copyright 2017, American Chemical Society.

4. CONCLUSION

This review has summarized recent advances in **polymer-based, ceramic-based, and hybrid PyNGs** as well as innovative application concepts.

- **Polymer-based PyNGs** (e.g., PVDF and copolymers) exhibit **flexibility, stretchability, and biocompatibility**, making them particularly suitable for **wearable electronics**.
- **Ceramic-based PyNGs** (e.g., BTO, BFO, $KNbO_3$, dabcoHReO4) possess **higher pyroelectric coefficients** and thus superior output performance, positioning them as strong candidates for **self-powered IoT systems**.

A comparative summary of key materials, pyroelectric coefficients, operational conditions, and performance metrics is presented in **Table 1**. Strategies such as **micropatterning, nanowire growth, and electrospun fibers**, as well as embedding ceramic nanoparticles in polymer matrices, have proven effective in enhancing both **flexibility and output efficiency**.

Nevertheless, several **critical challenges** remain before PyNGs can transition into large-scale applications:

1. **Environmental durability** – Long-term stability under repeated thermal cycling, solar irradiation, and high humidity is essential. Degradation of substrates or electrodes under such conditions could limit device lifetimes, even when pyroelectric materials themselves remain stable.

2. **Thermal limitations** – Pyroelectric activity is lost when operating temperatures exceed the material's **Curie temperature**, reducing reliability in harsh conditions.
3. **Power management** – High-efficiency harvesting requires **specialized nanoscale power management systems** to regulate output, minimize losses, and enable direct integration with IoT sensors.
4. **Material and structural innovation** – Continued progress in discovering **new pyroelectric materials**, reducing defects, and optimizing device architectures will be necessary to bridge the gap between theory and practice.

With systematic improvements in **material science, electronics, and thermal engineering**, PyNGs have the potential to evolve into **robust, multifunctional energy harvesters**, enabling **self-powered IoT platforms, smart building windows, wearable sensors, and environmental monitoring systems**. The combination of **flexibility, transparency, multifunctionality, and environmental safety** will make PyNGs a critical component of next-generation sustainable energy technologies.

REFERENCE:

[1] Zhang, T. (2020). Methods of improving the efficiency of thermal power plants. In *Journal of Physics: Conference Series* (Vol. 1449, No. 1, p. 012001). IOP Publishing.
[2] Rosen, M. A., & Bulucea, C. A. (2009). Using exergy to understand and improve the efficiency of electrical power technologies. *Entropy*, *11*(4), 820-835.
[3] Trinh, A. K., González, I., Fournier, L., Pelletier, R., & Lesage, F. J. (2014). Solar thermal energy conversion to electrical power. *Applied thermal engineering*, *70*(1), 675-686.
[4] Murehwa, G., Zimwara, D., Tumbudzuku, W., & Mhlanga, S. (2012). Energy efficiency improvement in thermal power plants. *International Journal of Innovative Technology and Exploring Engineering (IJITEE)*, *2*(1), 20-25.
[5] Li, Y., Samad, Y. A., Polychronopoulou, K., Alhassan, S. M., & Liao, K. (2014). From biomass to high performance solar–thermal and electric–thermal energy conversion and storage materials. *Journal of Materials Chemistry A*, *2*(21), 7759-7765.
[6] Soto, R., & Vergara, J. (2014). Thermal power plant efficiency enhancement with Ocean Thermal Energy Conversion. *Applied thermal engineering*, *62*(1), 105-112.
[7] Ryu, H., & Kim, S. W. (2021). Emerging pyroelectric nanogenerators to convert thermal energy into electrical energy. *Small*, *17*(9), 1903469.
[8] Cullen, J. M., & Allwood, J. M. (2010). Theoretical efficiency limits for energy conversion devices. *Energy*, *35*(5), 2059-2069.
[9] Maglogianni, M. E., Danoglidis, P. A., & Konsta-Gdoutos, M. S. (2023). Electrical-to-thermal energy conversion efficiency of conductive concrete. *Cement and Concrete Composites*, *139*, 104992.
[10] Lu, S., & Huang, Y. (2023). Graphene thermionic energy converter combined with an absorption heat transformer for electricity generation and thermal upgrading. *Applied Thermal Engineering*, *219*, 119640.
[11] Shen, Z. H., Ni, H., Ding, C., Sui, G. R., Jia, H. Z., Gao, X. M., & Wang, N. (2021). Improving the Energy-Conversion Efficiency of a PV–TE System With an Intelligent Power-Track Switching Technique and Efficient Thermal-Management Scheme. *IEEE Transactions on Components, Packaging and Manufacturing Technology*, *11*(6), 963-973.
[12] POPESCU, A., PANAITE, C. E., & STADOLEANU, O. V. (2013). Combined photovoltaic and thermal solar panels-enhanced energy conversion and heat transfer. *Termotehnica Supliment*, *1*.
[13] Zhang, E., Xu, C., Gao, Y., Zhu, X., Xie, Y., Xu, M., & Zhang, Y. (2025). An efficient ordered conversion system for hydrogen and electricity cogeneration driven by concentrated solar energy. *Applied Energy*, *377*, 124609.
[14] Virili, M., Georgiadis, A., Collado, A., Niotaki, K., Mezzanotte, P., Roselli, L., ... & Carvalho, N. B. (2015). Performance improvement of rectifiers for WPT exploiting thermal energy harvesting. *Wireless Power Transfer*, *2*(1), 22-31.
[15] Jiménez-Arreola, M., Pili, R., Dal Magro, F., Wieland, C., Rajoo, S., & Romagnoli, A. (2018). Thermal power fluctuations in waste heat to power systems: An overview on the challenges and current solutions. *Applied Thermal Engineering*, *134*, 576-584.
[16] Ma, Z., Mehos, M., Glatzmaier, G., & Sakadjian, B. B. (2015). Development of a concentrating solar power system using fluidized-bed technology for thermal energy conversion and solid particles for thermal energy storage. *Energy Procedia*, *69*, 1349-1359.